Both major xanthophyll cycles present in nature can provide Non-Photochemical Quenching in the model diatom *Phaeodactylum tricornutum*

Chiara E. Giossi[a]*, Marie A. Wünsch[a,c], Oliver Dautermann[b], Alexander F. Schober[a,d], Jochen M. Buck[a], Peter G. Kroth[a], Martin Lohr[b]*, Bernard Lepetit[a,c]*

[a] Department of Biology, University of Konstanz, 78464 Konstanz, Germany
[b] Institute of Molecular Physiology, Johannes Gutenberg University, 55099 Mainz, Germany
[c] Present address: Institute of Life Sciences, University of Rostock, 18059 Rostock, Germany
[d] Present address: School of Biological Science, Nanyang Technological University, 637551 Singapore

***To whom correspondence may be addressed:**

chiara.giossi@uni-konstanz.de, lohr@uni-mainz.de, bernard.lepetit@uni-rostock.de

Author Contributions: C.E.G. and B.L. designed the project; C.E.G., M.L. and B.L. designed experiments; A.F.S., M.A.W., and J.M.B. generated constructs for CRISPR-Cas KO and complementation lines; C.E.G., B.L. and M.A.W. generated and screened the mutant lines; C.E.G. performed experiments on *P. tricornutum* and analyzed the data; M.L. calculated and analyzed the xanthophyll cycle's kinetics. O.D. generated constructs for and performed the experiments on *Nicotiana plumbaginifolia*; C.E.G., M.A.W., P.G.K., M.L., and B.L. concluded the final data interpretation; C.E.G. wrote the initial draft of the manuscript, edited by B.L. and M.L.; The manuscript was revised and completed with contribution of all authors.

Competing Interest Statement: The authors declare no competing interest.

Classification: Biological Sciences, Plant Biology

Keywords: diatoms, non-photochemical quenching (NPQ), photoprotection, xanthophyll cycle

This PDF file includes:

Main Text
Figures 1 to 6

Abstract

Photosynthetic organisms require light but also rely on photoprotection to preempt photodamage induced by excess light. The xanthophyll cycle, a light-dependent carotenoid interconversion, plays a key role in the on- and offset of Non-Photochemical Quenching (NPQ), a form of excess energy dissipation through heat. While in most photosynthetic eukaryotes, including brown algae, green algae and plants, the violaxanthin cycle is prevalent, haptophytes and diatoms rely on the diadinoxanthin cycle to regulate NPQ. Diatoms also contain small amounts of violaxanthin cycle pigments, thought to serve only as precursors in xanthophylls biosynthesis. Both cycles are catalyzed by the enzymes violaxanthin de-epoxidase (VDE) and zeaxanthin epoxidase (ZEP). Here, we characterized the role of VDE and different ZEP encoding paralogs (*ZEP2* and *ZEP3*) in the model diatom *Phaeodactylum tricornutum*. We generated the respective knockout lines and treated exponentially growing mutants and wild type with periodic high light stress. We conclude that VDE and ZEP3 are the main regulators of the diadinoxanthin cycle. Under the same conditions, *ZEP2* knockouts accumulated mainly pigments of the violaxanthin cycle instead of the diadinoxanthin cycle. Intriguingly, violaxanthin cycle pigments contributed to the generation of NPQ with the same quenching efficiency of diadinoxanthin cycle pigments, demonstrating that both major xanthophyll cycles present in nature can provide NPQ in the same organism, with similar properties. Consequently, the prevalence of the diadinoxanthin cycle in diatoms has not been driven by its higher quenching efficiency but likely resulted from the selective advantage of a faster switch between photoprotection and light harvesting.

Significance Statement

Diatoms have a key role in almost any aquatic habitat, participate in nutrient cycling and contribute as much as the most productive terrestrial ecosystems to the global primary productivity. Diatoms are also regarded as biological factories of high value bioactive compounds, like carotenoids. Here, we investigated one of the most significant photoprotection mechanisms, the xanthophyll cycle, which relies on carotenoids to dissipate detrimental excess of light energy. Although diatoms use the so-called diadinoxanthin cycle, we discovered that the ancestral violaxanthin cycle, ubiquitous in plants and algae, can also contribute to photoprotection in these algae. We demonstrate that both cycles can function synergistically and with comparable efficiency within the same species, offering a new perspective on the evolution of xanthophyll-mediated photoprotection.

58 **Main Text**

59 **Introduction**

60 Diatoms are amongst the main primary producers on Earth (1, 2), dominating phytoplankton and
61 microphytobenthic communities in nutrient-rich turbulent waters (e.g., coasts and estuarine
62 mudflats) (3–5). In these habitats, light intensity can change very rapidly due to daily fluctuations
63 and to the movement of water and sediments (6). The temporary surplus of excitation energy
64 generated during these changes can be harmful to photosynthetic cells and generate reactive
65 oxygen species (ROS), resulting in photoinhibition (i.e., a decline of photosynthetic efficiency that
66 reduces growth and productivity) but also cellular oxidation and ultimately cell death (7). To thrive
67 under these complex conditions and cope with the highly dynamic light stress, diatoms have
68 evolved different photoprotection strategies (8, 9). One of these is Non-Photochemical Quenching
69 (NPQ), a ubiquitous multi-component mechanism that dissipates the surplus of excitation energy
70 as heat, thus preventing the over-saturation of the photosynthetic apparatus (10–13). The fastest
71 component of NPQ is known as qE, or high energy-state quenching, which takes place in the light-
72 harvesting complexes of photosystem II (PSII) (10–13). In diatoms, this process relies on antenna
73 proteins of the Lhcx family (14–17).
74 In most photosynthetic eukaryotes that lack phycobilisomes, the on- and offset of qE is regulated
75 by the xanthophyll cycle, a rapid interconversion of carotenoids that relies on removal or addition
76 of epoxy groups (18). Two major xanthophyll cycles exist in nature (12, 18): i) the violaxanthin (Vx)
77 cycle, a two-step reaction involving Vx, antheraxanthin (Ax) and zeaxanthin (Zx), present in green
78 algae, land plants and several classes of heterokont algae (such as brown algae, raphidophytes,
79 chrysophytes and eustigmatophytes); and ii) the diadinoxanthin (Dd) cycle, responsible for the
80 interconversion of only two pigments, Dd and diatoxanthin (Dt), found in haptophytes and other
81 heterokonts (such as diatoms, bolidophytes or pelagophytes). Both xanthophyll cycles are tightly
82 regulated via light-dependent changes in the thylakoidal ΔpH and control the on- and offset of qE
83 exclusively or synergistically with this ΔpH (12, 18). In diatoms, the light induced trans-thylakoid
84 ΔpH activates the enzyme violaxanthin de-epoxidase (VDE, also known as diadinoxanthin de-
85 epoxidase - DDE), converting Dd into Dt and thus triggering qE. When light stress and ΔpH are
86 relaxed, Dt is converted back to Dd by the enzyme zeaxanthin epoxidase (ZEP, also known as
87 diatoxanthin epoxidase - DEP), completing the cycle and thus abolishing qE (19, 20). Similarly, in
88 algae displaying the Vx cycle, qE is triggered by the de-epoxidation of Vx to Zx through the
89 intermediate Ax, and Vx is restored by the re-epoxidation of Zx (18).
90 Diatoms possess different paralogs of potential xanthophyll cycle enzymes that originated via
91 duplication of the respective ancestral genes (21, 22). In *Phaeodactylum tricornutum*, a
92 tychoplanktonic pennate diatom and the best-studied model organism of this group (23), multiple
93 paralogs of *VDE* (*VDE*, *VDL1*, *VDL2* and *VDR*) and *ZEP* (*ZEP1*, *ZEP2* and *ZEP3*) have been

identified (21). Recently, the role of ZEP1, VDL1 and VDL2 in the fucoxanthin biosynthetic pathway has been elucidated (24, 25). Hence, the photoprotective function must be provided by other paralogs such as *VDE*, *VDR, ZEP2* and/or *ZEP3*. Indeed, RNA silencing (26) and recombinant protein experiments (27, 28) pointed to VDE as the major regulator of Dd de-epoxidation in *P. tricornutum*. Moreover, *VDE* and *ZEP3* are arranged in a gene cluster conserved in *P. tricornutum* and other diatom lineages, suggesting shared evolutionary history and conserved functions (22, 25). Thus, VDE and ZEP3 could be the main regulators of the Dd cycle in *P. tricornutum*. On the contrary, ZEP2 may have an essential role in other photoprotection mechanisms and/or carotenoid biosynthesis (22, 29, 30).

Interestingly, diatoms and other algae using the Dd cycle can also accumulate pigments of the Vx cycle under extreme irradiance (30–32). The increase of Zx and Ax during prolonged high light, catalyzed by VDE, is explained by the essential role of Vx as intermediate in the biosynthesis of Dd and fucoxanthin (33, 34). However, it is unclear whether Zx and Ax can also trigger NPQ in diatoms.

In this work, we investigated the role of three xanthophyll cycle enzymes (ZEP2, ZEP3 and VDE) in the Dd and Vx cycle in *P. tricornutum* by generating respective knockout mutants. Our results highlight VDE and ZEP3 as major drivers of the Dd cycle: the VDE-deficient mutant (*vde KO*) was completely Dd cycle-deficient, while the ZEP3-deficient mutant (*zep3 KO*) did not rapidly re-epoxidize Dt after light stress. ZEP2-deficient mutants (*zep2 KO*) accumulated significantly large amounts of Zx and Ax under high light, at the expense of the Dd/Dt pool; nevertheless, their NPQ capacity was comparable to the *wild type* (wt). This proves that both major xanthophyll cycles present in nature can provide NPQ in the same organism and suggests that the prevalence of the Dd cycle in diatoms is not the result of Dt being superior to Zx in triggering qE.

Results

Genetic transformation of *P. tricornutum*. A CRISPR-Cas9 site directed mutagenesis approach was used to knockout *ZEP2*, *ZEP3* and *VDE*. We applied a combination of high-resolution melting curve (HRM) analysis and Sanger sequencing to identify clones with disrupted native gene (35). Induction-relaxation experiments were also performed in the preliminary screening phases to detect altered NPQ phenotypes. While *VDE* and *ZEP3* deficient lines showed a substantial lack of NPQ induction or recovery respectively, no clear phenotype alterations were observed for *ZEP2* deficient lines (**SI Appendix, Fig. S1**). Due to the diploid nature of *P. tricornutum* genome (36), the presence of knockout mutations on both alleles was finally assessed with TOPO cloning (**SI Appendix, Fig. S2**). We selected clones that harbored indels of varying lengths resulting in a disrupted gene on both alleles (**SI Appendix, Fig. S3**). Following sequential rounds of singularization to obtain monoclonality and promote the loss of the episome, resulting lines were

129 further confirmed with PCR genotyping (**SI Appendix, Fig. S4**). Additional information can be found
130 in **SI Appendix, Text S1**.

131 ***VDE*, *ZEP2* and *ZEP3* deficient mutants display characteristic pigment phenotypes in**
132 **response to high light (HL).** Under low light (LL), no major differences in pigment content were
133 observed between mutant lines and wt (**SI Appendix, Text S2, Table S2**). However, after 5 days
134 of 6 h HL:18 h LL regime each mutant displayed differences in xanthophyll cycling when compared
135 to wt (**Fig. 1**). In wt cells, Dd slightly decreased after 6h of HL, concomitant with a massive Dt
136 increase. In addition, minor amounts of Zx accumulated. During the following 30 min of recovery in
137 LL, Dt and Zx were almost entirely epoxidized back to Dd and Vx. As expected, *vde KO* did not
138 accumulate Dt or Zx during 6h of HL, but instead showed a strong increase of Dd and a small but
139 statistically significant increase in Vx. Conversely, *zep3 KO* accumulated the highest amount of Dt
140 under HL but was not able to convert it back to Dd during LL recovery. Finally, *zep2 KO* displayed
141 the Dd cycle in response to changing light, but these pigments were present in significantly lower
142 amounts compared to wt. Instead, this mutant was accumulating and cycling Vx cycle pigments to
143 a much higher extent than all other strains: Zx accumulated in response to 6h of HL and then
144 decreased during the early stages of recovery (5 min of LL), while a transient pool of Ax
145 accumulated; after 30min of LL, Vx accumulated at the expense of both Zx and Ax.
146 Additional information on the content of photosynthetic pigments is available as supporting
147 information (**SI Appendix, Fig. S5-7**). The phenotypes described for all mutants were reverted to
148 wt in mutant lines complemented with the respective native genes under native promoters (**SI**
149 **Appendix, Fig. S8-10**).

150 **All strains accumulate the same total pool of xanthophyll cycle pigments, but only *zep2 KO***
151 **displays the same proportion of de-epoxidized and epoxidized xanthophylls as wt.** After 6 h
152 of HL, all investigated lines approximatively tripled their total xanthophyll cycle pigment content,
153 with no significant difference between each mutant and wt (**Fig. 2C**). The amount of the light
154 harvesting xanthophyll fucoxanthin was not significantly altered (**SI Appendix, Fig. S7**). *vde KO*
155 and *zep3 KO* displayed no major difference in total Dd/Dt pool compared to wt (**Fig. 2A**), and in all
156 three lines the Vx cycle pool was almost absent (**Fig. 2B**). In contrast, *zep2 KO* displayed a much
157 lower Dd/Dt content (about 20% of the total xanthophyll cycle pigments, **Fig. 2A**) and instead
158 accumulated a massive total pool of Vx/Ax/Zx (about 80% of the total, **Fig. 2B**).
159 To further investigate the function-related accumulation of specific xanthophylls, we calculated the
160 total pool of epoxidized (**Fig. 2D**) and de-epoxidized pigments (**Fig. 2E**). In response to 6 h of HL,
161 *vde KO* accumulated a significantly higher amount of epoxidized xanthophylls, while these were
162 almost absent in *zep3 KO*. Instead, *zep3 KO* accumulated a significantly higher amount of de-
163 epoxidized pigments. Despite the strong differences in the individual amounts of Vx and Dd cycle

164 pigments (**Fig. 1**), *zep2 KO* did not display significant differences in the total pools of epoxidized or
165 de-epoxidized xanthophylls throughout the light treatments compared to wt (**Fig. 2E**).

166 **Despite a decreased Dd/Dt pool, *zep2 KO* displays wt-like NPQ capacity.** To investigate the
167 physiological effects of Vx/Ax/Zx accumulation in *zep2 KO*, the experiment was repeated with an
168 increased number of time points during recovery phase, and pigment analysis was coupled with
169 NPQ measurements. This confirmed the *zep2 KO* phenotype observed in the first set of
170 experiments (**Fig.1-2**), both in terms of xanthophyll cycle pigments (**Fig. 3A-E**) and total pools (**SI**
171 **Appendix, Fig. S9**). Additional time points allowed to better elucidate the Vx cycle kinetics (**Fig.**
172 **3C-E**): while Zx decreased immediately after the cultures were switched from HL to LL, Ax
173 transiently increased and reached its peak around 10 min of recovery, and then decreased in favor
174 of an increase of Vx.
175 Analysis of epoxidation kinetics during LL recovery (**Fig. 4**) showed that Zx and Dt were epoxidized
176 with similar rates within each algal strain, despite *zep2 KO* displayed lower rates for both reactions
177 compared to the wt. Again, *zep3 KO* showed hardly any epoxidation of Dt or Zx during the first 30
178 min of recovery (**SI Appendix, Fig. S12**) although a functional ZEP2 gene was present, as
179 evidenced by the regular formation of Vx-derived xanthophylls in this mutant. Transient expression
180 of *ZEP2* or *ZEP3* from *P. tricornutum* in the ZEP-deficient *aba2* mutant of *Nicotiana plumbaginifolia*
181 lacking epoxy xanthophylls resulted in almost identical pigment phenotypes accumulating Vx,
182 neoxanthin and lutein epoxide (**SI Appendix, Fig. S13**), indicating that both isoforms can accept
183 the same xanthophylls as substrate.
184 Despite a strongly reduced accumulation of Dd cycle pigments during HL (**Fig. 3A-B**), *zep2 KO* still
185 generated the same NPQ as wt (**Fig. 3F**). While NPQ relaxation was initially slower in the mutant,
186 no significant differences were observed after 30 min of recovery, indicating that *zep2 KO* was able
187 to relax its NPQ with an efficiency comparable to the wt. These results were confirmed with a
188 second independent *ZEP2* deficient mutant and a wt-like phenotype was restored for *zep2 KO* after
189 complementation with native *ZEP2* (**SI Appendix, Fig. S9-10**). The same analysis performed on
190 *zep3 KO* showed that the lack of Dt epoxidation during recovery directly corresponds to a lack of
191 NPQ relaxation and a persisting quenching state (**SI Appendix, Fig. S11**).

192 ***zep2 KO* and wt display the same linear correlation between pigment de-epoxidation and qE**
193 **when assuming the contribution of both xanthophyll cycles.** In most diatoms, NPQ linearly
194 correlates to the amount of Dt and this proportionality is especially robust when no significant
195 amounts of Vx cycle pigments are present (19, 20, 37). To factor in the presence of both distinct
196 pools of de-epoxidized xanthophylls, we performed five different calculations of the de-epoxidized

197 pigment pools possibly contributing to NPQ and analyzed their correlation with measured qE (**Fig.**
198 **5**).
199 Dt showed a clear linear relationship with qE in the wt (**Fig. 5A**), while this was much weaker in
200 *zep2 KO*. The opposite effect was observed with Zx (**Fig. 5B**), which yielded a better linear model
201 fit for *zep2 KO*. In both cases, wt and *zep2 KO* displayed a completely different correlation pattern,
202 noticeable by the poor fit of the combined linear model (i.e., including data points from both wt and
203 *zep2 KO*). With the sum of Dt and Zx (**Fig. 5C**), model fit improved and the slopes of the linear
204 regression for wt and mutant began to converge. However, a strong linear correlation was observed
205 only in the wt. The linear fit significantly improved when summing Dt, Zx and ½ Ax (**Fig. 5D**): models
206 for both *zep2 KO* and wt converged towards the general linear model, with the highest R^2 values.
207 This indicates that the size of this specific pigment pool correlates with qE in a similar manner
208 between these strains. Moreover, the addition of the full Ax pool (**Fig. 5E**) yielded a poorer fit for all
209 investigated lines (with a notable decrease in R^2 values). We conclude that the sum of Dt, Zx and
210 ½ Ax most adequately describes the xanthophyll cycle-dependent component of NPQ in HL-
211 acclimated *P. tricornutum*.
212 We further confirmed these results with a second *ZEP2* deficient mutant and complementation of
213 *zep2 KO* with native *ZEP2* (**SI Appendix, Fig. S14**).

214 **Discussion**

215 **VDE and ZEP3 are the key players in the Dd cycle in *P. tricornutum*.** Our first set of experiments
216 (**Fig. 1-2**) confirmed VDE and ZEP3 as main enzymes of photoprotective xanthophyll cycling in *P.*
217 *tricornutum*: *vde KO* accumulated only Dd and was not able to de-epoxidize it to Dt in response to
218 light stress; conversely, *zep3 KO* was unable to rapidly re-epoxidize Dt into Dd shortly after a light
219 stress (i.e., during recovery phase), which resulted in a permanent quenching state, as confirmed
220 by analyses of NPQ and xanthophyll kinetics (**SI Appendix, Fig. S11-12**). Previously, ZEP2 had
221 been indicated as main candidate for driving Dt epoxidation, based on a strong accumulation of
222 monoepoxides (Ax and lutein epoxide) in a ZEP-deficient *npq2* mutant of *Arabidopsis thaliana*
223 stably transformed with *ZEP2* from *P. tricornutum* (38). Our results however demonstrate that ZEP3
224 is the ZEP isoform mainly co-regulating the Dd cycle with VDE in *P. tricornutum*. This is consistent
225 with the clustered organization of *VDE* and *ZEP3* within the genomes of *P. tricornutum* and various
226 other diatoms (21, 22, 25) and with several reports of their correlated expression pattern under light
227 stress (9, 21, 30, 39).
228 Although *zep3 KO* accumulated high amounts of Dt during HL, the mutant was almost devoid of Dt
229 before the onset of HL on the 5th day of light stress regime (**Fig. 1**, Time = 0 h), indicating that Dt
230 epoxidation could still be performed in this mutant on longer time scales. ZEP2 and ZEP3 from *P.*
231 *tricornutum* showed similarly broad substrate specificities in tobacco (**SI Appendix, Fig. S13**),
232 suggesting that both isoforms should allow epoxidation of Zx as well as Dt. ZEP2 is thus likely

233 responsible for the long-term re-epoxidation of Dt and Zx in *zep3 KO* following HL exposure,
234 although hardly any epoxidation activity was detectable during the first 30 min of recovery. A major
235 contribution of carotenoid degradation to the scavenging of Dt in the *zep3 KO* during prolonged LL
236 recovery appears unlikely, since carotenoid catabolism is known to be stimulated under higher
237 irradiances (40, 41).

238 **The Vx cycle can function as NPQ catalyst in *P. tricornutum*.** After 6 h of HL, *zep2 KO* displayed
239 wt-like NPQ (**Fig. 3B**) despite a much smaller Dt pool along with a compensatory increase of Vx
240 cycle pigments (**Fig. 1-3**). Including Zx and Ax in the linear model between qE and de-epoxidized
241 pigments resulted in a fit comparable to that of the wt (**Fig. 5**). The best linear fit was achieved
242 when qE was modelled against the sum of Dt, Zx and ½ Ax, suggesting that both Zx and Ax can
243 induce NPQ, with the latter having only around half of the quenching capacity of Zx and Dt.
244 Ax is known to participate in NPQ in various other photosynthetic eukaryotes. Early studies on the
245 Vx cycle in plants indicated Zx as the pigment with quenching activity (42, 43), but soon the
246 additional involvement of Ax was reported (44–47). Ax is thought to participate in quenching also
247 in green lineage algae, with taxon-specific differences (e.g. *Chlorella vulgaris* (48), *Mantoniella*
248 *squamata* (49)). In the heterokont *Nannochloropsis oceanica*, Ax also contributes to qE with about
249 30% efficiency compared to Zx (50). Moreover, in the giant kelp *Macrocystis pyrifera*, Ax
250 participates in quenching with half of the efficiency observed for Zx (51). Brown algae only possess
251 the Vx cycle (52) but display diatom-like qE (i.e., relying directly on the xanthophyll cycle while not
252 being activated by ∆pH alone (53)), likely explaining the similarities with our findings for
253 *P. tricornutum*.
254 The major mediators of qE in diatoms are Lhcx proteins, that likely bind Dd/Dt (16, 54–56), as the
255 structurally and functionally related LhcSR proteins of *C. reinhardtii* bind Vx cycle pigments (57).
256 Various other proteins related to light harvesting also bind xanthophyll cycle pigments in diatoms
257 (58–60). Xanthophylls are known to compete for different binding sites within the antennae (61–
258 64), and mutants lacking one pigment can substitute it with a closely related one (e.g., in *A. thaliana*
259 (65, 66) and *C. reinhardtii* (67)). As it is established that Dd/Dt must be bound to light harvesting
260 proteins to provide NPQ (68, 69), we propose that Vx, Ax and Zx, when accumulated in favorable
261 concentrations, could occupy the same binding sites thus contributing to qE induction, as indicated
262 by our data (**Fig. 3-5**). This suggests that Dt might be equally able to confer NPQ as Zx/Ax do in
263 taxa that normally rely on the Vx cycle. Once the yet unknown Dd synthase (24) is discovered, this
264 hypothesis could be tested by implementing the Dd biosynthesis pathway in the green lineage.
265 Vx and Dd cycle pigments differ only due to a triple bond within the isoprenoid backbone of Dd and
266 Dt (**Fig. 1**). This renders the central polyene moiety asymmetrical, in contrast to the symmetric Vx
267 cycle counterparts. Due to this asymmetry, Dd and Dt may be directionally inserted into the
268 antennae binding sites, with the Vx cycle-like half of the molecule (corresponding to the epoxy/de-
269 epoxidized group) interacting with the quenching-related site (17, 59). In contrast, Vx, Ax and Zx

270 might access the quenching site in either orientation due to the perfect symmetry of their polyene
271 moiety. This would result in a 50% chance of Ax being oriented with its epoxidized or de-epoxidized
272 ionone ring towards the quenching site, potentially explaining why our analyses suggest that Ax
273 has about half of the quenching capacity of Zx and Dt.

274 ***De novo* synthesis is responsible for the light-induced accumulation of photoprotective**
275 **xanthophylls.** Although the xanthophyll cycle pool was permanently epoxidized in *vde KO* and de-
276 epoxidized in *zep3 KO*, the total amount of xanthophyll cycle pigments accumulating during HL was
277 the same in both mutants and wt (**Fig. 2**). Even *zep2 KO* accumulated the same total amount of
278 xanthophylls under HL, although this was driven mostly by an increase of Zx/Ax. This suggests that
279 the rate of de-novo biosynthesis of carotenoids is not affected by any of the target mutations, thus
280 being likely regulated in the same way in all investigated lines.
281 Previous studies suggested that *de novo* synthesis from β-carotene is responsible for the high light
282 induced accumulation of Zx in *P. tricornutum* (31), as in other algae (e.g., *Chlamydomonas*
283 *reinhardtii* (70)). Accordingly, we observed no significant differences in fucoxanthin content under
284 different light conditions between all investigated mutants and wt (**SI Appendix, Text S2, Fig. S7**).
285 This indicates that this pigment is most likely not converted back into photoprotective xanthophylls
286 under light stress and thus confirms that *de novo* synthesis is responsible for the xanthophyll cycle
287 pools increase observed during high light.

288 **Functional diversification of ZEP2 and ZEP3 uncouples *de novo* xanthophyll biosynthesis**
289 **from xanthophyll cycling.** Most land plants and green algae encode only a single ZEP that
290 participates in photoprotective xanthophyll cycling and in *de novo* biosynthesis of Vx and its
291 derivatives (12, 21). Under HL, these organisms accumulate newly synthesized carotenoids mainly
292 as Zx, which supports NPQ. In diatoms and other algae with the Dd cycle, Vx is an obligate
293 precursor of Dd and fucoxanthin (24, 25, 31). Dt is then synthesized from Dd by VDE. Therefore,
294 *de novo* Dt biosynthesis under HL requires the activity of both ZEP (that epoxidizes new Zx to Vx)
295 and VDE (that generates Dt from Dd). As both enzymes work in opposite directions, this could
296 potentially result in a futile cycle. This apparent paradox is solved by dynamic tuning of VDE and
297 ZEP activity (20). Compared to the green lineage, in diatoms VDE becomes active at a less acidic
298 pH (71–73) and requires a lower amount of the co-factor ascorbate (74, 75), while epoxidation is
299 much faster but is almost completely switched off under higher irradiance by yet unknown
300 mechanisms (19, 20). ZEP has been proposed as the main regulator of xanthophyll cycling and
301 NPQ in diatoms and other closely related taxa (20, 76), but the role of the different isoforms was
302 not elucidated. In our study, differences between *zep2 KO* and *zep3 KO* clearly indicate that the
303 corresponding enzymes carry out non-redundant functions, as previously speculated in gene
304 expression studies (21). Our data suggest that despite the two isoforms share some properties,

305 *P. tricornutum* splits the functions of photoprotective xanthophyll cycling and *de novo* biosynthesis
306 of carotenoids between ZEP2 and ZEP3.
307 As discussed above, all our strains displayed similarly high rates of *de novo* xanthophyll synthesis
308 during HL. The strong increase of Dd/Dt in both wt and *zep3 KO* indicates a sustained epoxidase
309 activity under HL, which must be supplied by ZEP2. On the other hand, ZEP3 appears to be
310 switched off under higher irradiance (19, 20) (**Fig. 1** and **SI Appendix, Fig. S12**), preventing the
311 epoxidation of VDE-generated Dt (and Zx) and ensuring the onset of NPQ (**Fig. 3**). Similarly, ZEP
312 inactivation under extreme irradiances has been postulated in *Nannochloropsis gaditana*, an
313 heterokont displaying only the Vx cycle (77). We therefore conclude that in *P. tricornutum* ZEP3 is
314 active exclusively under non-saturating irradiances to rapidly tune down NPQ, while ZEP2 has
315 properties closer to the ZEP of higher plants and green algae, i.e., a constant activity under all
316 irradiance condition (including darkness and HL) (45, 48, 49, 78). Consequently, in *zep2 KO* the
317 lack of ZEP2 in combination with the inactivation of ZEP3 and the increased VDE activity under HL
318 results in the accumulation of Zx/Ax (**Fig. 1-2**). A strong VDE activity competing with Dd formation
319 would also explain why accumulation of Vx/Ax/Zx can be observed to some extent in the wt under
320 extreme irradiances (**Fig. 1-3**) (30–32). This scenario is illustrated in **Fig. 6A**.
321 Alternatively, our results could be explained by a spatial separation of the two ZEP paralogs in the
322 plastids, as previously proposed (32). According to this model (**Fig. 6B**) ZEP2 would be mostly
323 confined to the inner plastid envelope, while ZEP3 would be mainly located at the thylakoid
324 membranes. ZEP2 would thus be responsible for the epoxidation of Zx to Vx during *de novo*
325 carotenoid biosynthesis in the envelope. Vx would then be transported to the thylakoid membranes
326 for further conversion to Dd and fucoxanthin. Conversely, ZEP3 would be responsible for
327 xanthophyll cycle-related Dt epoxidation, in accordance with the wt-like epoxidation rates and NPQ
328 (**Fig. 3-5**) observed in our *zep2 KO*. In absence of ZEP2, carotenoid biosynthesis in the envelopes
329 would already cease at the level of Zx which would be translocated to the thylakoid membranes
330 instead of Vx where it could participate in quenching under HL and be epoxidized to Vx by ZEP3
331 in subsequent LL. This model allows to assume a considerably higher epoxidase activity for ZEP2
332 in the envelope than the experimentally determined epoxidation rates of Dt and Zx located in the
333 thylakoid membranes (32, 33).
334 In conclusion, both functional specialization (**Fig. 6A**) and/or spatial separation (**Fig. 6B**) could
335 contribute to uncouple *de novo* xanthophyll synthesis from xanthophyll cycling in *P. tricornutum*.

336 **Evolutionary implications of Vx cycling in diatoms.** Xanthophyll cycling is thought to represent
337 an innovation of eukaryotic oxygenic phototrophs, and to have evolved in parallel with light
338 harvesting and other photoprotection strategies (21, 79). The Dd cycle most probably evolved in
339 an alga that already possessed the Vx cycle, as Vx is an obligate precursor of Dd and fucoxanthin
340 (24, 25, 31) and VDE and ZEP have sufficiently broad substrate specificities for accepting the
341 xanthophylls from both cycles as substrates (27, 28, 80). According to this scenario, both

342 xanthophyll cycles were functional in the same organism during the early evolution of
343 photosynthetic heterokonts. Extant algae with Dd cycle still have the potential to accumulate the
344 pigments of the Vx cycle (31) which, however, is effectively suppressed under most conditions.
345 One explanation for the prevalence of the Dd cycle in these algae could be that Dt is more effective
346 than Zx in triggering NPQ. Our observation that the Vx cycle pigments can efficiently provide NPQ
347 in a modern diatom species that normally relies solely on the Dd cycle rejects this hypothesis, while
348 it supports the idea of a gradual shift in photoprotection from the Vx to the Dd cycle in heterokont
349 algae.
350 Replacing the two-step Vx cycle with the one-step Dd cycle provides the benefit of switching faster
351 between photosynthetic light harvesting and NPQ (19, 31, 81). Moreover, the formation of
352 fucoxanthin involves only 5 enzymatic steps from Dt versus 8 steps from Zx (25, 82), thereby also
353 accelerating the conversion of photoprotective xanthophylls accumulated under higher irradiance
354 into light harvesting pigments when light becomes limited. The selective advantage conferred by
355 these factors likely also contributed to the success of diatoms in dynamic ecosystem such as
356 turbulent waters that are characterized by frequent and extreme light changes (6).

357 **Materials and Methods**

358 **CRISPR/Cas9-based gene knockout.** *Phaeodactylum tricornutum* (Pt1; CCAP1055) maintained
359 for several years in our laboratory was used as reference wt and for the generation of all mutant
360 strains. Independent knockout lines (two for ZEP2 [Phatr2_56488; chr_1:2222646-2224755(+)],
361 and one for VDE [Phatr2_44635; chr_4:1116193-1117626(-)] and ZEP3 [Phatr2_56492;
362 chr_4:1118248-1120587(+)]) were obtained with CRISPR/Cas9 genome editing, through bacterial
363 conjugation. sgRNAs were designed with CRISPOR (83) and episomal vectors based on
364 pPtPuc3m diaCas9_sgRNA including the respective sgRNA templates were created following
365 previously published methods (35, 84). sgRNA coding sequences can be found in **SI Appendix,**
366 **Table S3**. Final episomes (containing CRISPR/Cas9 machinery and zeocin resistance cassette)
367 were first transformed into *E. coli* DH10β cells carrying the mobilization helper plasmid pTA-Mob
368 and further introduced into wtPt1 *via* bacterial conjugation, as previously described (84–86).
369 Transformed clones appeared 2-3 weeks after conjugation on agar selection plates (16 g/L salinity
370 f/2 + 100 µg/mL zeocin) incubated at 20°C and 100 µmol photons m^{-2} s^{-1} of white light and were
371 transferred on fresh selection plates (16 g/L salinity f/2 agar + 75 µg/mL zeocin). Screening of
372 mutants followed the strategy previously described (35) and included pre-screening of potentially
373 mutated DNA sequences by PCR amplification via DreamTaq (ThermoFisher Scientific Inc.,
374 Germany) and high-resolution melting curve analysis (HRM) using Biozym HRM PCR Mix (Biozym
375 Scientific GmbH, Germany); primers are listed in **SI Appendix, Table S1**. NPQ phenotypes of the
376 putative mutants were also screened through a chlorophyll *a* fluorescence induction-relaxation
377 protocol (5-10 min light stress at 500-600 µmol photons m^{-2} s^{-1} with blue light, followed by recovery

378 at 28 µmol photons m^{-2} s^{-1}) performed with an IMAGING-PAM fluorometer (IMAG-C model with
379 IMAG-K camera, Heinz Walz GmbH, Germany). For this purpose, cultures were inoculated in well
380 plates with liquid media (16 g/L salinity f/2 + 50 µg/mL zeocin) and grown for 3-4 days at 100 µmol
381 photons m^{-2} s^{-1} of white light.
382 After identification of positive candidates, the isolation and screening procedure was repeated 1-3
383 times to obtain pure monoclonal cultures. We confirmed the mutation in both alleles and the
384 monoclonality of the colonies using TOPO-TA cloning (ThermoFisher Scientific Inc., Germany)
385 followed by sequencing of the individual alleles. Mutated clones with a KO indel on both alleles
386 were selected for experiments. Additional information is available in **SI Appendix, Text S1**.
387 KO mutants were maintained for several months at 16 °C and 25 µmol photons m^{-2} s^{-1} of white light
388 with 16:8 h light:dark photoperiod on 16 g/L salinity f/2 agar plates without antibiotic selection, to
389 facilitate the expulsion of the CRISPR/Cas9 episome. In addition, prolonged cultivation of
390 transgenic lines was necessary to achieve a stable phenotype before performing experiments, as
391 it is known that in *P. tricornutum* the effects of mutations can be alleviated via compensatory
392 mechanisms such as upregulation of other genes (87). All KO strains generated for this study were
393 later cryopreserved according to (88).

394 **Complementation of mutant lines.** For each targeted gene (*VDE*, *ZEP2*, and *ZEP3*) we created
395 a modified pPTbsr vector containing the whole length wt gene (amplified from gDNA) with predicted
396 endogenous promoter and terminator to achieve wt-like gene expression. To avoid targeting of the
397 newly inserted sequence, synonymous mutations were introduced at the site of the protospacer
398 adjacent motif in *ZEP2* and *ZEP3*, while a selected episome-free *vde* mutant strain was used for
399 complementation with *VDE*. Biolistic transformation was performed according to (89).
400 Transformants were grown on selection plates (8 g/L salinity f/2 agar + 4 µg/mL blasticidin-S) for
401 1-3 weeks at 20°C with 100 µmol photons m^{-2} s^{-1} of white light. DNA of selected clones was
402 extracted as described in (35) and PCR was performed with ALLin™ Mega HiFi DNA Polymerase
403 (highQu GmbH, Germany). PCR products were sequenced (Microsynth, Balgach, Switzerland) and
404 clones showing the insertion of the complete target gene were selected. Primers are listed in **SI**
405 **Appendix, Table S4**. Complementation lines were then cryopreserved according to (88).

406 **PCR genotyping.** In absence of a commercial antibody for our target proteins, PCR genotyping
407 with high discrimination polymerase (HiDi, MyPols, Germany) was performed to confirm the purity
408 of all selected lines prior experiments. gDNA was extracted with the same protocol described for
409 transformants screening (35) and amplification was performed according to manufacturer's
410 instructions (with addition of 1 mM $MgCl_2$), using allele-discriminating primers flanking the targeting
411 loci and binding specifically in each line (KO, wt and complemented). Two different primer pairs
412 were used to confirm the presence of both mutated alleles (allele 1 and allele 2) in the KO lines.
413 Primers are listed in **SI Appendix, Table S1**. PCR products were run on 1% or 2% TAE-agarose

414 gels with 1000 bp or 50 bp GeneRuler (ThermoFisher Scientific Inc., Germany) depending on
415 product size. All gels were stained with ROTI GelStain (Roth Gmbh, Germany). Additional
416 information is available in **SI Appendix, Text S1**.

417 **Culture conditions.** All experimental strains were maintained in a temperature-controlled growth
418 chamber at 18°C in shaking batch cultures (120-150 rpm). Standard f/2 medium (90) was prepared
419 with 16 g/L Tropic Marine CLASSIC sea salt (Dr. Biener GmbH, Germany) adjusted to 7.5 pH prior
420 autoclaving. Continuous low light (LL, 30-50 $\mu mol_{photons}$ m^{-2} s^{-1}), measured in culture flask filled with
421 f/2 medium with a ULM-500 light meter with spherical sensor (Heinz Walz GmbH, Germany), was
422 supplied with L 18W/954 LUMILUX® DELUXE Daylight tubes (OSRAM GmbH, Germany).
423 About one week prior to each experiment, cultures were acclimated to semi-chemostatic conditions
424 at 18 °C and continuous LL. For the whole experiment, cultures were maintained at 1-2*10^6 cells/mL
425 in semi-chemostat by daily dilution with fresh medium based on cell counts (Multisizer 4e coulter
426 counter, BECKMAN COULTER, USA).

427 **Experimental setup.** Semi-chemostat cultures acclimated to LL were treated for 5 consecutive
428 days with 6 h of high light (HL, 1000-1200 µmol photons m^{-2} s^{-1} measured in f/2 medium,
429 corresponding to ~700 µmol photons m^{-2} s^{-1} in air as used by (31), supplied by HO 80W/865
430 LUMILUX® Cool Daylight, OSRAM GmbH, Germany), followed by 18 h of LL. For pigments
431 analysis, samples were harvested before (LL control) and after 5 days of HL:LL treatment. At the
432 fifth day, cultures were sampled before the onset of the 6 h HL phase (0 h), after 6 h of HL and
433 during recovery in LL (5 and 30 min). Samples (5 mL) were vacuum filtered (ISOPORE™ 1.2 µm
434 PC membrane filters, 25 mm), flash-frozen in liquid nitrogen and stored at -80 °C for later analysis
435 with HPLC.
436 To investigate the correlation between the kinetics of xanthophyll cycling and NPQ, the experiment
437 was repeated on *zep* mutants and wt. This time, pigment analysis was coupled with fluorescence
438 measurements: at the fifth day of HL:LL treatment, chlorophyll fluorescence was measured, using
439 an IMAGING-PAM fluorometer (IMAG-C model with IMAG-K camera, Heinz Walz GmbH,
440 Germany), immediately before the 6 h HL phase (0 h), after 6 h of HL and in the following LL phase
441 after 1, 3, 5, 7.5, 10, 15 and 30 min. Samples (3 mL) were collected from the shaking Erlenmeyer
442 flasks and immediately transferred into a 24-well plate that was positioned below the IMAGING-
443 PAM, but still received the same experimental light (LL or HL) as the Erlenmeyer flasks during the
444 measurement. A saturating pulse of blue light (max intensity: 3000 µmol photons m^{-2} s^{-1}; width: 800
445 ms) was applied to measure Fm/Fm'. Simultaneously, samples (5 mL) were collected from the
446 same Erlenmeyer flasks for pigment analysis and preserved as described above. This approach
447 allowed to determine a precise pigment-NPQ correlation under our experimental conditions. NPQ
448 (Fm-Fm′/Fm′) was derived defining Fm obtained at the first LL pulse (0 h) (91). To isolate its effect
449 from the photoinhibition-related quenching (qI), qE (i.e., the rapidly relaxing component of NPQ,

450 also indicated as qZ in diatoms) was calculated as Fm''-Fm'/Fm', where Fm'' corresponds to the
451 maximum fluorescence at the end of the recovery phase (30 min) (20). Similarly, corresponding Δs
452 for xanthophyll cycle pigments were calculated as [p]-[p]'', where [p] corresponds to the pigment
453 concentration at a given time point, and [p]'' at the end of the recovery phase (30 min).

454 **Pigment analysis (HPLC).** Pigments extraction was performed as in (16). Samples (80 µL) were
455 separated on a NUCLEOSIL® C18 column (EC 250/4, 300-5, MACHEREY-NAGEL GmbH,
456 Germany) in a LaChrome Elite HPLC equipped with an L-2130 pump module, L-2455 diode array
457 detector, and L-2200 autosampler (VWR International, Germany). Elution was performed at 0.8
458 mL/min flow rate using a three-phase gradient consisting of eluent A (85% methanol, 15% 0.5M
459 ammonium acetate in water), B (90% acetonitrile, 10% water), and C (100% ethyl acetate) following
460 the protocol established by (92). Classical diatom pigments were identified from known absorption
461 spectra and retention times (93) and quantified using the integrated absorption peak area at 440
462 nm and previously determined conversion factors. Retention times and λ_{max} for each pigment and
463 representative chromatograms for each mutant are reported in **SI Appendix, Table S2, Fig. S5**.
464 For Vx cycle pigments, preliminary identification was further confirmed via spiking with pure
465 crystalline standards (DHI group, Hørsholm, Denmark). If detected, content of chlorophyllide *a* was
466 always summed to that of chlorophyll *a*. Preliminary data assessment was performed with
467 EZChrome *Elite* (Agilent, USA) and OpenChrome (Lablicate Gmbh, Germany) (94).

468 **Transient expression of *P. tricornutum ZEP2* and *ZEP3* in a ZEP-deficient tobacco mutant.**
469 Full-length *ZEP2* and *ZEP3* from *P. tricornutum* strain UTEX 646 were PCR-amplified from cDNA
470 using Phusion High-Fidelity DNA Polymerase (Thermo Scientific, Carlsbad, USA) and subcloned
471 into the pGEM-T® Easy Vector (Promega, Mannheim, Germany). PCR-related mutations were
472 excluded by confirming that sequences of the cloned genes were identical to sequencing results
473 from PCR products. For generation of plasmids for *Agrobacterium*-mediated tobacco
474 transformation, the gene fragments encoding the mature proteins were PCR amplified, subcloned
475 into pGEM®-T Easy, excised with AvrII and PacI and ligated into the AvrII and PacI sites of plasmid
476 pPZPbar-tp_{AtZEP}-AtZEP (95), thereby replacing the ZEP gene from *Arabidopsis thaliana* and
477 yielding plasmids pPZPbar-tp_{AtZEP}-PtZEP2 and pPZPbar-tp_{AtZEP}-PtZEP3. Growth of the ZEP-
478 deficient *aba2* mutant of tobacco *N. plumbaginifolia* (Marin et al., 1996), the *Agrobacterium*-
479 mediated transformation of tobacco leaves with the pPZPbar constructs of *AtZEP*, *PtZEP2* and
480 *PtZEP3*, sampling and pigment analysis of lyophilized tobacco leaf discs was performed as
481 described before (95). All analyses were done at least in triplicate from independent transformants,
482 with the HPLC chromatograms showing representative results.

483 **Data analysis and statistics.** DNA and protein sequences were analyzed with Geneious 9.1
484 (Biomatters, New Zealand, 2016). Analysis of pigment and chlorophyll *a* fluorescence data was

performed with R 4.2.1 (R foundation for statistical computing, Vienna, Austria). Multiple comparison t-tests were performed to test differences in average pigment content and NPQ between mutant lines and wt at different time points; adjusted p-values (Holm correction for multiple comparisons) were used to evaluate statistical significance. Normality was evaluated prior with a combination of graphical methods (Q-Q plot, residual analysis) and Shapiro-Wilk test. For qE/Δpigment correlations, linear regressions were modeled with a standard linear model function. Model fit was evaluated with graphical methods (Q-Q plot, residual analysis) and R^2. Finally, xanthophyll cycle kinetics were manually fitted in Microsoft Excel using first order kinetics equations (96); for each time point, molar ratios of pigment/chlorophyll *a* were normalized to the total pool size of each xanthophyll cycle individually.

Acknowledgments

C.E.G. thanks the Studienstiftung des Deutschen Volkes (Bonn, Germany) for her doctoral scholarship. BL thanks the DFG (LE 3358/3-2) and Heisenberg program. The authors acknowledge Benjamin Bailleul for his support in NPQ modelling. We also thank Annette Ramsperger for her contribution to the generation of mutant lines, and Alexander H. Fürst, Selina Pucher and Manuel Müller for their help during preliminary characterization and genotyping of the mutants, in the aim of a practical course. Finally, C.E.G thanks Prof. David Schleheck for the project discussions.

Data and strains availability statement

Mutant algal strains are cryopreserved in the laboratory of Prof. Peter Kroth (Department of Biology, University of Konstanz, 78457 Konstanz, Germany) and are available upon request. Additional queries can be addressed to the corresponding authors.

References

1. C. B. Field, M. J. Behrenfeld, J. T. Randerson, P. G. Falkowski, Primary Production of the Biosphere: Integrating Terrestrial and Oceanic Components. *Science (1979)* **281**, 237–240, (1998).

2. P. G. Falkowski, *et al.*, The evolution of modern eukaryotic phytoplankton. *Science (1979)* **305**, 354–360, (2004).

3. C. Barranguet, J. Kromkamp, J. Peene, Factors controlling primary production and photosynthetic characteristics of intertidal microphytobenthos. *Mar Ecol Prog Ser* **173**, 117–126, (1998).

4. G. F. Blanchard, J. M. Guarini, C. Dang, P. Richard, Characterizing and quantifying photoinhibition in intertidal microphytobenthos. *J Phycol* **40**, 692–696, (2004).

517 5. S. Tozzi, O. Schofield, P. G. Falkowski, Historical climate change and ocean turbulence
518 as selective agents for two key phytoplankton functional groups. *Mar Ecol Prog Ser* **274**,
519 123–132, (2004).

520 6. J. Lavaud, Fast Regulation of Photosynthesis in Diatoms: Mechanisms, Evolution and
521 Ecophysiology. *Functional Plant Science and Biotechonology* **1**, 267–287, (2007).

522 7. M. A. Gururani, J. Venkatesh, L. S. P. Tran, Regulation of photosynthesis during abiotic
523 stress-induced photoinhibition. *Mol Plant* **8**, 1304–1320, (2015).

524 8. J. Lavaud, R. F. Strzepek, P. G. Kroth, Photoprotection capacity differs among diatoms:
525 Possible consequences on the spatial distribution of diatoms related to fluctuations in the
526 underwater light climate. *Limnol Oceanogr* **52**, 1188–1194, (2007).

527 9. C. Kan, Y. Zhao, K. Sun, X. Tang, Y. Zhao, The inhibition and recovery mechanisms of
528 the diatom *Phaeodactylum tricornutum* in response to high light stress - A study combining
529 physiological and transcriptional analysis. *J Phycol*, (2023),
530 https:/doi.org/10.1111/jpy.13323.

531 10. S. Takahashi, M. R. Badger, Photoprotection in plants: a new light on photosystem II
532 damage. *Trends Plant Sci* **16**, 53–60, (2011).

533 11. N. Domingues, A. R. Matos, J. M. da Silva, P. Cartaxana, Response of the Diatom
534 *Phaeodactylum tricornutum* to photooxidative stress resulting from high light exposure.
535 *PLoS One* **7**, (2012).

536 12. R. Goss, B. Lepetit, Biodiversity of NPQ. *J Plant Physiol* **172**, 13–32, (2015).

537 13. R. Bassi, L. Dall'Osto, Dissipation of Light Energy Absorbed in Excess: The Molecular
538 Mechanisms. *Annu Rev Plant Biol* **72**, 47–76, (2021).

539 14. B. Bailleul, *et al.*, An atypical member of the light-harvesting complex stress-related
540 protein family modulates diatom responses to light. *Proc Natl Acad Sci U S A* **107**, 18214–
541 18219, (2010).

542 15. B. Lepetit, *et al.*, The diatom *Phaeodactylum tricornutum* adjusts nonphotochemical
543 fluorescence quenching capacity in response to dynamic light via fine-tuned Lhcx and
544 xanthophyll cycle pigment synthesis. *New Phytologist* **214**, 205–218, (2017).

545 16. J. M. Buck, *et al.*, Lhcx proteins provide photoprotection via thermal dissipation of
546 absorbed light in the diatom *Phaeodactylum tricornutum*. *Nat Commun* **10**, (2019).

547 17. J. M. Buck, P. G. Kroth, B. Lepetit, Identification of sequence motifs in Lhcx proteins that
548 confer qE-based photoprotection in the diatom *Phaeodactylum tricornutum*. *The Plant*
549 *Journal* **108**, 1721–1734, (2021).

550 18. D. Latowski, P. Kuczyńska, K. Strzałka, Xanthophyll cycle – a mechanism protecting
551 plants against oxidative stress. *Redox Report* **16**, 78–90, (2011).

552 19. R. Goss, E. Ann Pinto, C. Wilhelm, M. Richter, The importance of a highly active and ΔpH-
553 regulated diatoxanthin epoxidase for the regulation of the PS II antenna function in
554 diadinoxanthin cycle containing algae. *J Plant Physiol* **163**, 1008–1021, (2006).

555 20. L. Blommaert, L. Chafai, B. Bailleul, The fine-tuning of NPQ in diatoms relies on the
556 regulation of both xanthophyll cycle enzymes. *Sci Rep* **11**, 1–16, (2021).

557 21. S. Coesel, M. Oborník, J. Varela, A. Falciatore, C. Bowler, Evolutionary origins and
558 functions of the carotenoid biosynthetic pathway in marine diatoms. *PLoS One* **3**, (2008).

22. R. Frommolt, *et al.*, Ancient recruitment by chromists of green algal genes encoding enzymes for carotenoid biosynthesis. *Mol Biol Evol* **25**, 2653–2667, (2008).

23. A. De Martino, A. Meichenin, J. Shi, K. Pan, C. Bowler, Genetic and phenotypic characterization of *Phaeodactylum tricornutum* (Bacillariophyceae) accessions. *J Phycol* **43**, 992–1009, (2007).

24. O. Dautermann, *et al.*, An algal enzyme required for biosynthesis of the most abundant marine carotenoids. *Sci Adv* **6**, (2020).

25. Y. Bai, *et al.*, Green diatom mutants reveal an intricate biosynthetic pathway of fucoxanthin. *Proceedings of the National Academy of Sciences* **119**, (2022).

26. J. Lavaud, A. C. Materna, S. Sturm, S. Vugrinec, P. G. Kroth, Silencing of the violaxanthin de-epoxidase gene in the diatom *Phaeodactylum tricornutum* reduces diatoxanthin synthesis and non-photochemical quenching. *PLoS One* **7**, (2012).

27. M. Olchawa-Pajor, M. Bojko, W. Strzalka, K. Strzalka, D. Latowski, Violaxanthin conversion by recombinant diatom and plant de-epoxidases, expressed in *Escherichia coli* – a comparative analysis. *Acta Biochim Pol* **66**, 249–255, (2019).

28. M. Bojko, *et al.*, Expression of three diadinoxanthin de-epoxidase genes of *Phaeodacylum tricornutum* in *Escherichia coli* Origami b and BL21 strain. *Acta Biochim Pol* **60**, 857–60, (2013).

29. C. Wilhelm, *et al.*, The Regulation of Carbon and Nutrient Assimilation in Diatoms is Significantly Different from Green Algae. *Protist* **157**, 91–124, (2006).

30. P. Kuczynska, *et al.*, The xanthophyll cycle in diatom *Phaeodactylum tricornutum* in response to light stress. *Plant Physiology and Biochemistry* **152**, 125–137, (2020).

31. M. Lohr, C. Wilhelm, Algae displaying the diadinoxanthin cycle also possess the violaxanthin cycle. *Proc Natl Acad Sci U S A* **96**, 8784–8789, (1999).

32. M. Lohr, C. Wilhelm, Xanthophyll synthesis in diatoms: quantification of putative intermediates and comparison of pigment conversion kinetics with rate constants derived from a model. *Planta* **212**, 382–391, (2001).

33. M. Lohr, “Carotenoid metabolism in phytoplankton” in *Phytoplankton Pigments*, Cambridge Environmental Chemistry Series., S. Roy, C. Llewellyn, E. S. Egeland, G. Johnsen, Eds. (Cambridge University Press, 2011), , pp. 113–162.

34. M. Dambek, *et al.*, Biosynthesis of fucoxanthin and diadinoxanthin and function of initial pathway genes in *Phaeodactylum tricornutum*. *J Exp Bot* **63**, 5607–5612, (2012).

35. M. Nymark, *et al.*, CRISPR/Cas9 Gene Editing in the Marine Diatom *Phaeodactylum tricornutum*. *Bio Protoc* **7**, 1–12, (2017).

36. C. Bowler, *et al.*, The Phaeodactylum genome reveals the evolutionary history of diatom genomes. *Nature* **456**, 239–244, (2008).

37. D. Croteau, *et al.*, Contrasting nonphotochemical quenching patterns under high light and darkness aligns with light niche occupancy in Arctic diatoms. *Limnol Oceanogr* **66**, S231–S245, (2021).

38. U. Eilers, L. Dietzel, J. Breitenbach, C. Büchel, G. Sandmann, Identification of genes coding for functional zeaxanthin epoxidases in the diatom *Phaeodactylum tricornutum*. *J Plant Physiol* **192**, 64–70, (2016).

601 39. M. Nymark, *et al.*, An integrated analysis of molecular acclimation to high light in the
602 marine diatom *Phaeodactylum tricornutum*. *PLoS One* **4**, (2009).

603 40. B. Biswal, Carotenoid catabolism during leaf senescence and its control by light. *J*
604 *Photochem Photobiol B* **30**, 3–13, (1995).

605 41. S. Steiger, L. Schäfer, G. Sandmann, High-light-dependent upregulation of carotenoids
606 and their antioxidative properties in the cyanobacterium *Synechocystis* PCC 6803. *J*
607 *Photochem Photobiol B* **52**, 14–18, (1999).

608 42. B. Demmig-Adams, Carotenoids and photoprotection in plants: A role for the xanthophyll
609 zeaxanthin. *Biochimica et Biophysica Acta (BBA) - Bioenergetics* **1020**, 1–24, (1990).

610 43. E. Pfündel, W. Bilger, Regulation and possible function of the violaxanthin cycle.
611 *Photosynth Res* **42**, 89–109, (1994).

612 44. A. M. Gilmore, H. Y. Yamamoto, Linear models relating xanthophylls and lumen acidity to
613 non-photochemical fluorescence quenching. Evidence that antheraxanthin explains
614 zeaxanthin-independent quenching. *Photosynth Res* **35**, 67–78, (1993).

615 45. A. M. Gilmore, N. Mohanty, H. Y. Yamamoto, Epoxidation of zeaxanthin and
616 antheraxanthin reverses non-photochemical quenching of photosystem II chlorophyll a
617 fluorescence in the presence of trans-thylakoid ΔpH. *FEBS Lett* **350**, 271–274, (1994).

618 46. B. Demmig-Adams, W. W. Adams, The role of xanthophyll cycle carotenoids in the
619 protection of photosynthesis. *Trends Plant Sci* **1**, 21–26, (1996).

620 47. J. Zaks, K. Amarnath, E. J. Sylak-Glassman, G. R. Fleming, Models and measurements of
621 energy-dependent quenching. *Photosynth Res* **116**, 389–409, (2013).

622 48. R. Goss, B. Lepetit, C. Wilhelm, Evidence for a rebinding of antheraxanthin to the light-
623 harvesting complex during the epoxidation reaction of the violaxanthin cycle. *J Plant*
624 *Physiol* **163**, 585–590, (2006).

625 49. R. Goss, K. Böhme, C. Wilhelm, The xanthophyll cycle of *Mantoniella squamata* converts
626 violaxanthin into antheraxanthin but not to zeaxanthin: consequences for the mechanism
627 of enhanced non-photochemical energy dissipation. *Planta* **205**, 613–621, (1998).

628 50. A. Short, *et al.*, Kinetics of the xanthophyll cycle and its role in photoprotective memory
629 and response. *Nat Commun* **14**, (2023).

630 51. H. Ocampo-Alvarez, E. García-Mendoza, Govindjee, Antagonist effect between
631 violaxanthin and de-epoxidated pigments in nonphotochemical quenching induction in the
632 qE deficient brown alga *Macrocystis pyrifera*. *Biochim Biophys Acta Bioenerg* **1827**, 427–
633 437, (2013).

634 52. E. García-Mendoza, M. F. Colombo-Pallotta, The giant kelp Macrocystis pyrifera presents
635 a different nonphotochemical quenching control than higher plants. *New Phytologist* **173**,
636 526–536, (2007).

637 53. J. Lavaud, R. Goss, "The Peculiar Features of Non-Photochemical Fluorescence
638 Quenching in Diatoms and Brown Algae" in *Non-Photochemical Quenching and Energy*
639 *Dissipation in Plants, Algae and Cyanobacteria*, B. Demmig-Adams, G. Garab, W. Adams
640 III, Govindjee, Eds. (Springer Dordrecht, 2014), , pp. 421–443.

641 54. L. Taddei, *et al.*, Dynamic changes between two LHCX-related energy quenching sites
642 control diatom photoacclimation. *Plant Physiol* **177**, 953–965, (2018).

643 55. B. Lepetit, *et al.*, “Photosynthetic Light Reactions in Diatoms. II. The Dynamic Regulation
644 of the Various Light Reactions” in *The Molecular Life of Diatoms*, A. Falciatore, T. Mock,
645 Eds. (Springer International Publishing, 2022), , pp. 423–464.

646 56. S. Zhao, *et al.*, Structural insights into photosystem II supercomplex and trimeric FCP
647 antennae of a centric diatom *Cyclotella meneghiniana*. *Nat Commun* **14**, (2023).

648 57. G. Bonente, *et al.*, Analysis of LHcSR3, a protein essential for feedback de-excitation in
649 the green alga *Chlamydomonas reinhardtii*. *PLoS Biol* **9**, (2011).

650 58. B. Lepetit, D. Volke, M. Gilbert, C. Wilhelm, R. Goss, Evidence for the existence of one
651 antenna-associated, lipid-dissolved and two protein-bound pools of diadinoxanthin cycle
652 pigments in diatoms. *Plant Physiol* **154**, 1905–1920, (2010).

653 59. W. Wang, *et al.*, Structural basis for blue-green light harvesting and energy dissipation in
654 diatoms. *Science (1979)* **363**, (2019).

655 60. R. Nagao, *et al.*, Structural basis for different types of hetero-tetrameric light-harvesting
656 complexes in a diatom PSII-FCPII supercomplex. *Nat Commun* **13**, (2022).

657 61. R. Croce, S. Weiss, R. Bassi, Carotenoid-binding sites of the major light-harvesting
658 complex II of higher plants. *Journal of Biological Chemistry* **274**, 29613–29623, (1999).

659 62. S. Hobe, H. Niemeier, A. Bender, H. Paulsen, Carotenoid binding sites in LHCIIb. *Eur J*
660 *Biochem* **267**, 616–624, (2000).

661 63. S. Caffarri, R. Croce, J. Breton, R. Bassi, The major antenna complex of Photosystem II
662 has a xanthophyll binding site not involved in light harvesting. *Journal of Biological*
663 *Chemistry* **276**, 35924–35933, (2001).

664 64. V. Mascoli, *et al.*, Uncovering the interactions driving carotenoid binding in light-harvesting
665 complexes. *Chem Sci* **12**, 5113–5122, (2021).

666 65. L. Dall’Osto, S. Cazzaniga, H. North, A. Marion-Poll, R. Bassi, The *Arabidopsis* aba4-1
667 mutant reveals a specific function for neoxanthin in protection against photooxidative
668 stress. *Plant Cell* **19**, 1048–1064, (2007).

669 66. L. Kalituho, J. Rech, P. Jahns, The roles of specific xanthophylls in light utilization. *Planta*
670 **225**, 423–439, (2007).

671 67. F. Azadi-Chegeni, *et al.*, Protein dynamics and lipid affinity of monomeric, zeaxanthin-
672 binding LHCII in thylakoid membranes. *Biophys J* **121**, 396–409, (2022).

673 68. V. Giovagnetti, *et al.*, Biochemical and molecular properties of LHCX1, the essential
674 regulator of dynamic photoprotection in diatoms. *Plant Physiol* **188**, 509–525, (2022).

675 69. A. Schumann, R. Goss, T. Jakob, C. Wilhelm, Investigation of the quenching efficiency of
676 diatoxanthin in cells of *Phaeodactylum tricornutum* (Bacillariophyceae) with different pool
677 sizes of xanthophyll cycle pigments. *Phycologia* **46**, 113–117, (2007).

678 70. I. Baroli, A. D. Do, T. Yamane, K. K. Niyogi, Zeaxanthin accumulation in the absence of a
679 functional xanthophyll cycle protects *Chlamydomonas reinhardtii* from photooxidative
680 stress. *Plant Cell* **15**, 992–1008, (2003).

681 71. H. Y. Yamamoto, “[34] Xanthophyll cycles” in *Steroids and Isoprenoids, Part A*, Methods in
682 Enzymology., (Academic Press, 1985), , pp. 303–312.

683 72. T. Jakob, R. Goss, C. Wilhelm, Unusual pH-dependence of diadinoxanthin de-epoxidase
684 activation causes chlororespiratory induced accumulation of diatoxanthin in the diatom
685 *Phaeodactylum tricornutum*. *J Plant Physiol* **158**, 383–390, (2001).

686 73. C. Fufezan, D. Simionato, T. Morosinotto, Identification of key residues for pH dependent
687 activation of violaxanthin de-epoxidase from *Arabidopsis thaliana*. *PLoS One* **7**, (2012).

688 74. C. E. Bratt, P.-O. Arvidsson, M. Carlsson, H.-E. Åkerlund, Regulation of violaxanthin de-
689 epoxidase activity by pH and ascorbate concentration. *Photosynth Res* **45**, 169–175,
690 (1995).

691 75. I. Grouneva, T. Jakob, C. Wilhelm, R. Goss, Influence of ascorbate and pH on the activity
692 of the diatom xanthophyll cycle-enzyme diadinoxanthin de-epoxidase. *Physiol Plant* **126**,
693 205–211, (2006).

694 76. N. Berne, T. Fabryova, B. Istaz, P. Cardol, B. Bailleul, The peculiar NPQ regulation in the
695 stramenopile *Phaeomonas* sp. challenges the xanthophyll cycle dogma. *Biochim Biophys*
696 *Acta Bioenerg* **1859**, 491–500, (2018).

697 77. G. Perin, *et al.*, Modulation of xanthophyll cycle impacts biomass productivity in the marine
698 microalga *Nannochloropsis*. *Proceedings of the National Academy of Sciences* **120**,
699 (2023).

700 78. D. Siefermann, H. Y. Yamamoto, NADPH and oxygen-dependent epoxidation of
701 zeaxanthin in isolated chloroplasts. *Biochem Biophys Res Commun* **62**, 456–461, (1975).

702 79. E. Garcia-Mendoza, H. Ocampo-Alvarez, Govindjee, Photoprotection in the brown alga
703 *Macrocystis pyrifera*: Evolutionary implications. *J Photochem Photobiol B* **104**, 377–385,
704 (2011).

705 80. H. Y. Yamamoto, R. M. Higashi, Violaxanthin de-epoxidase: Lipid composition and
706 substrate specificity. *Arch Biochem Biophys* **190**, 514–522, (1978).

707 81. J. Lavaud, B. Rousseau, A.-L. Etienne, In diatoms, a transthylakoid proton gradient alone
708 is not sufficient to induce a non-photochemical fluorescence quenching. *FEBS Lett* **523**,
709 163–166, (2002).

710 82. T. Cao, *et al.*, An unexpected hydratase synthesizes the green light-absorbing pigment
711 fucoxanthin. *Plant Cell*, (2023), https:/doi.org/10.1093/plcell/koad116.

712 83. J. P. Concordet, M. Haeussler, CRISPOR: Intuitive guide selection for CRISPR/Cas9
713 genome editing experiments and screens. *Nucleic Acids Res* **46**, W242–W245, (2018).

714 84. A. K. Sharma, M. Nymark, T. Sparstad, A. M. Bones, P. Winge, Transgene-free genome
715 editing in marine algae by bacterial conjugation – comparison with biolistic CRISPR/Cas9
716 transformation. *Sci Rep* **8**, 1–11, (2018).

717 85. B. J. Karas, *et al.*, Designer diatom episomes delivered by bacterial conjugation. *Nat*
718 *Commun* **6**, (2015).

719 86. R. E. Diner, V. A. Bielinski, C. L. Dupont, A. E. Allen, P. D. Weyman, Refinement of the
720 diatom episome maintenance sequence and improvement of conjugation-based DNA
721 delivery methods. *Front Bioeng Biotechnol* **4**, (2016).

722 87. M. Nymark, *et al.*, Functional studies of CpSRP54 in diatoms show that the mechanism of
723 thylakoid protein insertion differs from that in plants and green algae. *Plant Journal* **106**,
724 113–132, (2021).

88. B. N. Sprecher, *et al.*, Genetic transformation methods for diatom *Nitzschia captiva*: New tools to better understand dinotom endosymbiosis. *Algal Res* **72**, 103136, (2023).

89. P. G. Kroth, “Genetic Transformation” in *Protein Targeting Protocols*, M. van der Giezen, Ed. (Humana Press, 2007), , pp. 257–267.

90. R. R. L. Guillard, “Culture of Phytoplankton for Feeding Marine Invertebrates” in *Culture of Marine Invertebrate Animals*, (Springer US, 1975), , pp. 29–60.

91. E. H. Murchie, T. Lawson, Chlorophyll fluorescence analysis: A guide to good practice and understanding some new applications. *J Exp Bot* **64**, 3983–3998, (2013).

92. G. W. Kraay, M. Zapata, M. J. W. Veldhuis, Separation of chlorophylls *c1*, *c2*, and *c3* of marine phytoplankton by reversed-phase C18 high-performance liquid chromatography. *J Phycol* **28**, 708–712, (1992).

93. S. Roy, C. Llewellyn, E. S. Egeland, G. Johnsen, *Phytoplanton Pigments - Characterization, Chemotaxonomy and Applications in Oceanography Pigments* (Cambridge University Press, 2011).

94. P. Wenig, J. Odermatt, OpenChrom: A cross-platform open source software for the mass spectrometric analysis of chromatographic data. *BMC Bioinformatics* **11**, (2010).

95. O. Dautermann, M. Lohr, A functional zeaxanthin epoxidase from red algae shedding light on the evolution of light-harvesting carotenoids and the xanthophyll cycle in photosynthetic eukaryotes. *Plant Journal* **92**, 879–891, (2017).

96. K. J. Laidler, *Reaction Kinetics* (Elsevier Science & Technology, 1970).

Figures

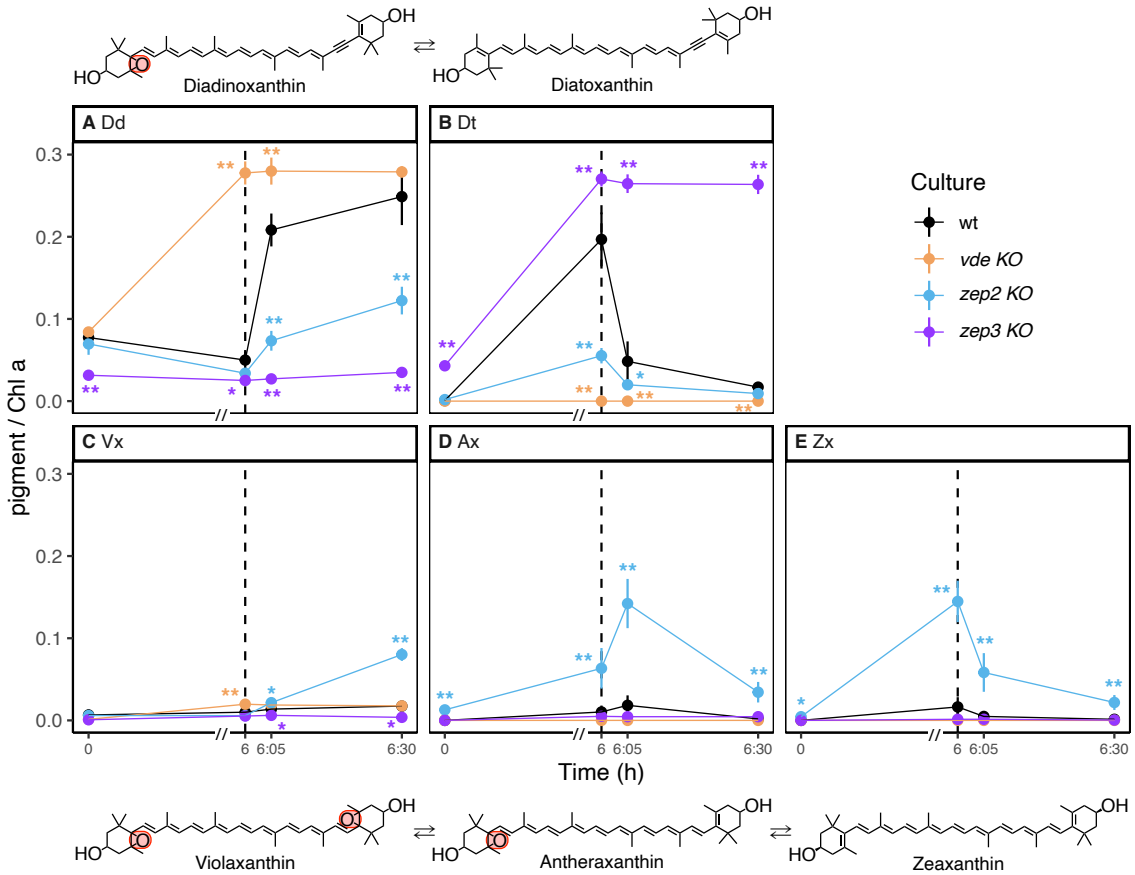

Fig. 1. Content of Dd and Vx cycle pigments in wt, *vde KO*, *zep2 KO* and *zep3 KO* after 5 days of HL:LL regime (average ± sd, n=3). Pigment content is expressed as pigment:chlorophyll *a* ratio (mol/mol). The 6 h of HL phase and 30 min of recovery phase (LL) are separated with a dashed line. On the x-axis, recovery phase (from 6 to 6:30 h) was artificially enlarged to allow better visualization; axis break is indicated by a double dash (//). (*A*) diadinoxanthin; (*B*) diatoxanthin; (*C*) violaxanthin; (*D*) antheraxanthin; (*E*) zeaxanthin. Epoxy groups are highlighted with a red rectangle. Statistical significance marks indicate significant differences between the corresponding mutant line and wt at each time point, according to adjusted p-value of multiple comparison t-test (*: $p < 0.05$; **: $p < 0.005$).

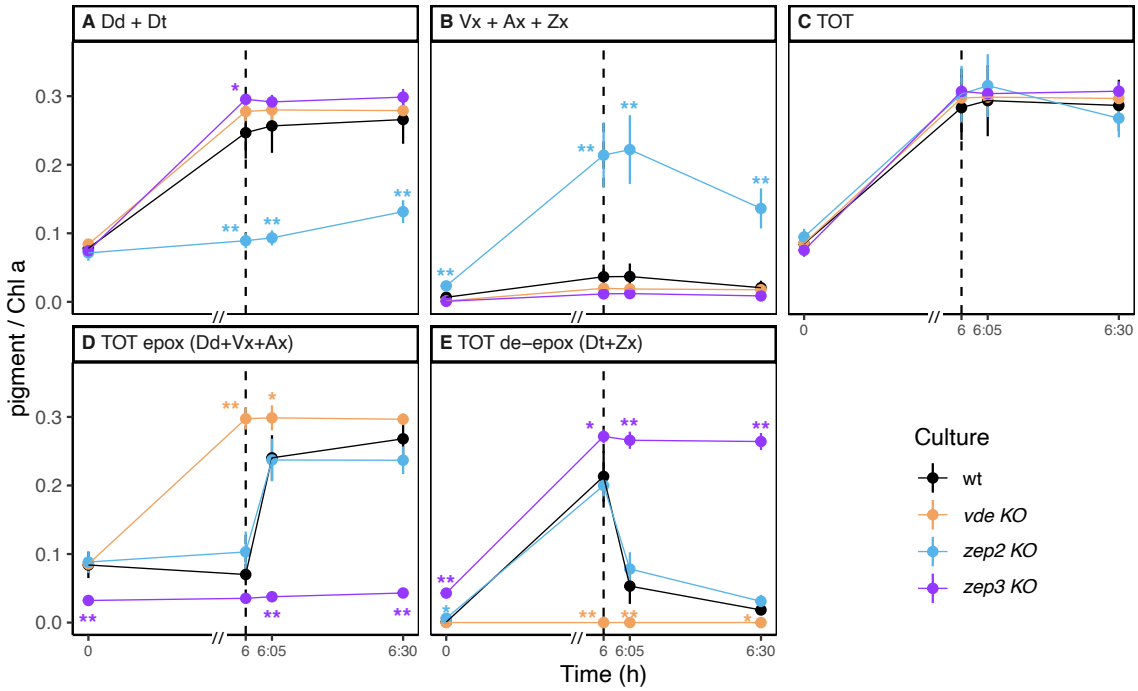

758

759 **Fig. 2. Total pools of Dd and Vx cycle pigments in wt, *vde KO*, *zep2 KO* and *zep3 KO* after 5**
760 **days of HL:LL regime (average ± sd, n=3).** Pigment content is expressed as pigment:chlorophyll
761 *a* ratio (mol/mol). The 6 h of HL phase and 30 min of recovery phase (LL) are separated with a
762 dashed line. On the x-axis, recovery phase (from 6 to 6:30 h) was artificially enlarged to allow better
763 visualization; axis break is indicated by a double dash (//). (*A*) total pool of Dd cycle pigments
764 (diadinoxanthin + diatoxanthin); (*B*) total pool of Vx cycle pigments (violaxanthin + antheraxanthin
765 + zeaxanthin); (*C*) sum of all Dd and Vx cycle pigments; (*D*) total pool of epoxidized pigments
766 across different xanthophyll cycles (diadinoxanthin + violaxanthin + antheraxanthin); (*E*) total pool
767 of de-epoxidized pigments across different xanthophyll cycles (diatoxanthin + zeaxanthin).
768 Statistical significance marks indicate significant differences between the corresponding mutant
769 line and wt at each time point, according to adjusted p-value of multiple comparison t-test (*: $p < 0.05$; **: $p < 0.005$).
770

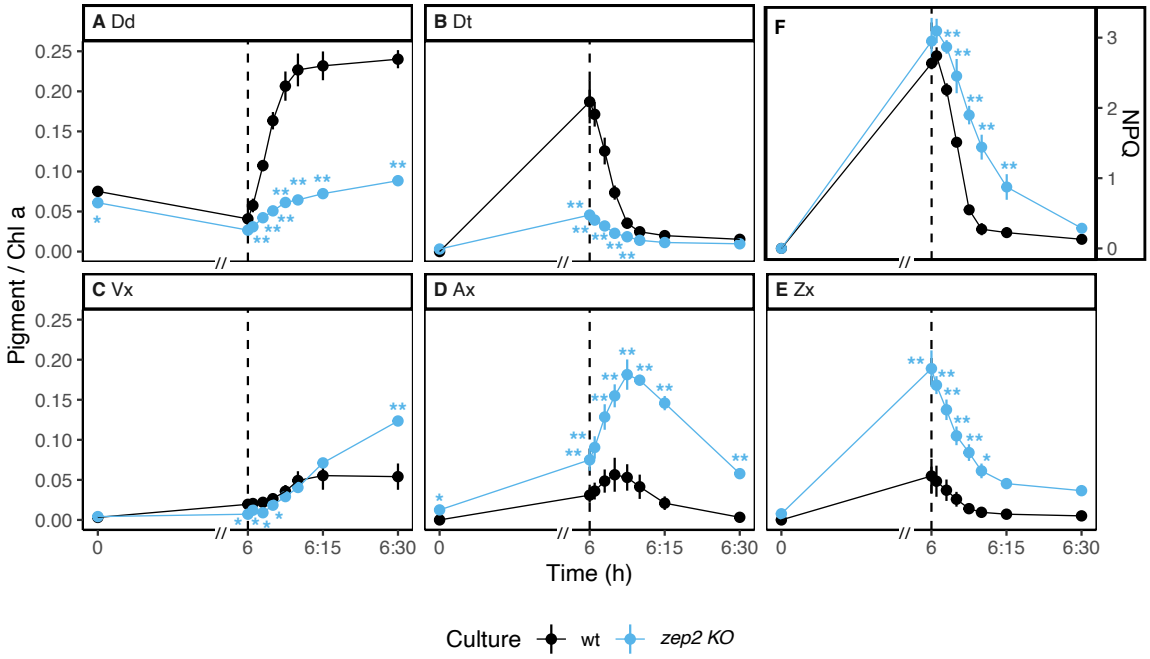

771

772 **Fig. 3. Pigment content of Dd and Vx cycle pigments coupled with NPQ analysis in wt and**
773 ***zep2 KO* after 5 days of HL:LL regime (average ± sd, n=3).** Pigment content is expressed as
774 pigment:chlorophyll *a* ratio (mol/mol). The 6 h of HL phase and 30 min of recovery phase (LL) are
775 separated with a dashed line. On the x-axis, recovery phase (from 6 to 6:30 h) was artificially
776 enlarged to allow better visualization; axis break is indicated by a double dash (*//*). (*A*)
777 diadinoxanthin; (*B*) diatoxanthin; (*C*) violaxanthin; (*D*) antheraxanthin; (*E*) zeaxanthin; (*F*) NPQ.
778 Statistical significance marks indicate significant differences between the corresponding mutant
779 line and wt at each time point, according to adjusted p-value of multiple comparison t-test (*: $p < 0.05$; **: $p < 0.005$).
780

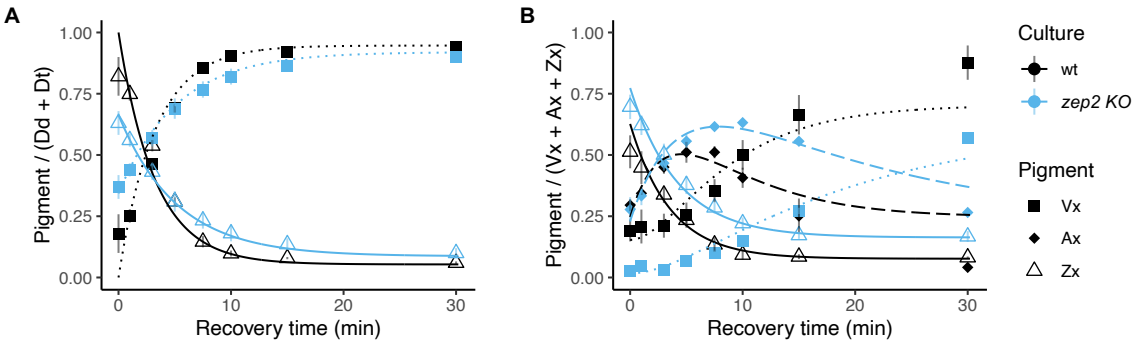

C

	Dt → Dd	Zx → Ax	Ax → Vx	Ratios					
	k_T [min^{-1}]	k_Z [min^{-1}]	k_A [min^{-1}]	k_T/k_Z	k_Z/k_T	k_T/k_A	k_A/k_T	k_Z/k_A	k_A/k_Z
wt	0.310 ± 0.017	0.280 ± 0.035	0.167 ± 0.076	1.11 ± 0.08	0.90 ± 0.06	2.10 ± 0.81	0.53 ± 0.22	1.87 ± 0.61	0.58 ± 0.22
zep2 KO	0.193 ± 0.012	0.237 ± 0.015	0.058 ± 0.003	0.82 ± 0.02	1.22 ± 0.03	3.31 ± 0.03	0.30 ± 0.003	4.06 ± 0.10	0.25 ± 0.01

Fig. 4. First order kinetics of re-epoxidation of xanthophyll cycle pigments in wt and *zep2 KO* during 30 min of recovery phase after HL (average ± sd, n=3). (*A*) epoxidation of diadinoxanthin (Dd) to diatoxanthin (Dt); (*B*) epoxidation of zeaxanthin (Zx) via antheraxanthin (Ax) to violaxanthin (Vx); (*C*) corresponding rate constants of epoxidation.

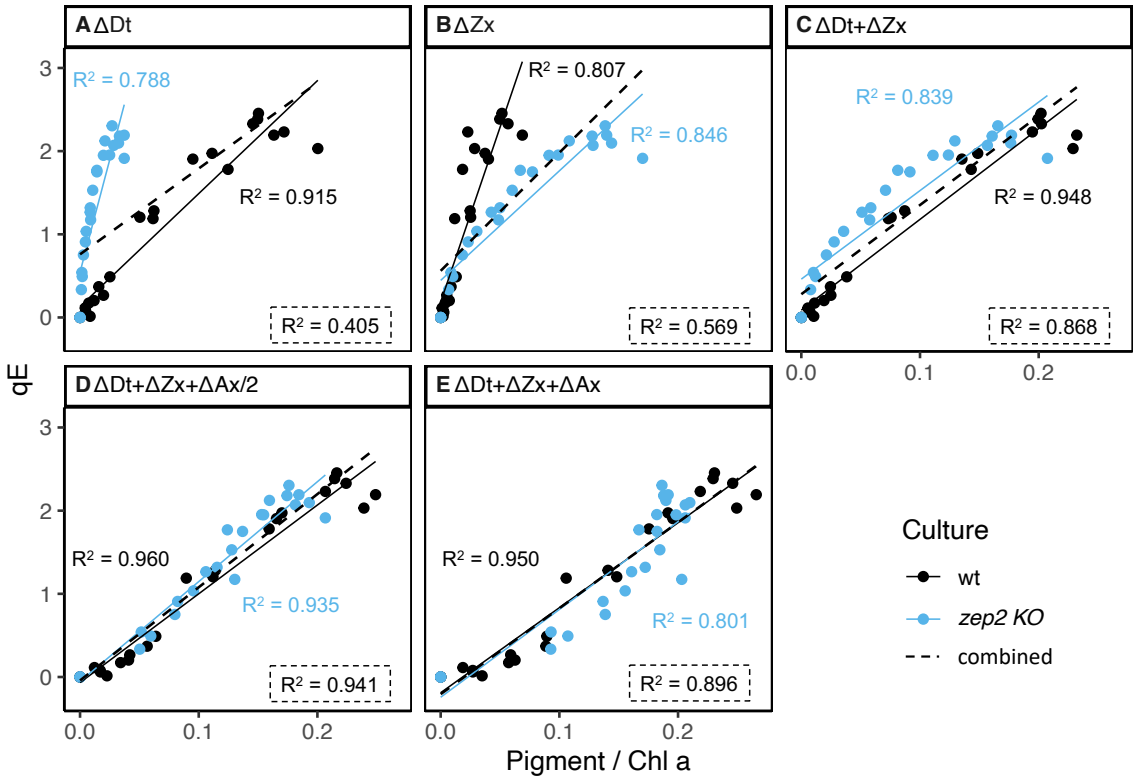

Fig. 5. Correlation between qE and de-epoxidized pigments in wt and *zep2 KO* during recovery from 6 h of HL, on the 5th day of HL:LL exposure. Each point represents a separate measurement, repeated for 3 independent biological replicates. For each strain, different calculations of de-epoxidized pigment pool are displayed, with corresponding linear models and R^2. Dashed lines represent the linear model obtained when considering *zep2 KO* and wt as one unique population (combined); corresponding R^2 is displayed in the dashed text box at the bottom right corner of each facet. (*A*) diadinoxanthin only; (*B*) zeaxanthin only; (*C*) diatoxanthin and zeaxanthin; (*D*) diatoxanthin, zeaxanthin and ½ antheraxanthin; (*E*) diatoxanthin, zeaxanthin and antheraxanthin.

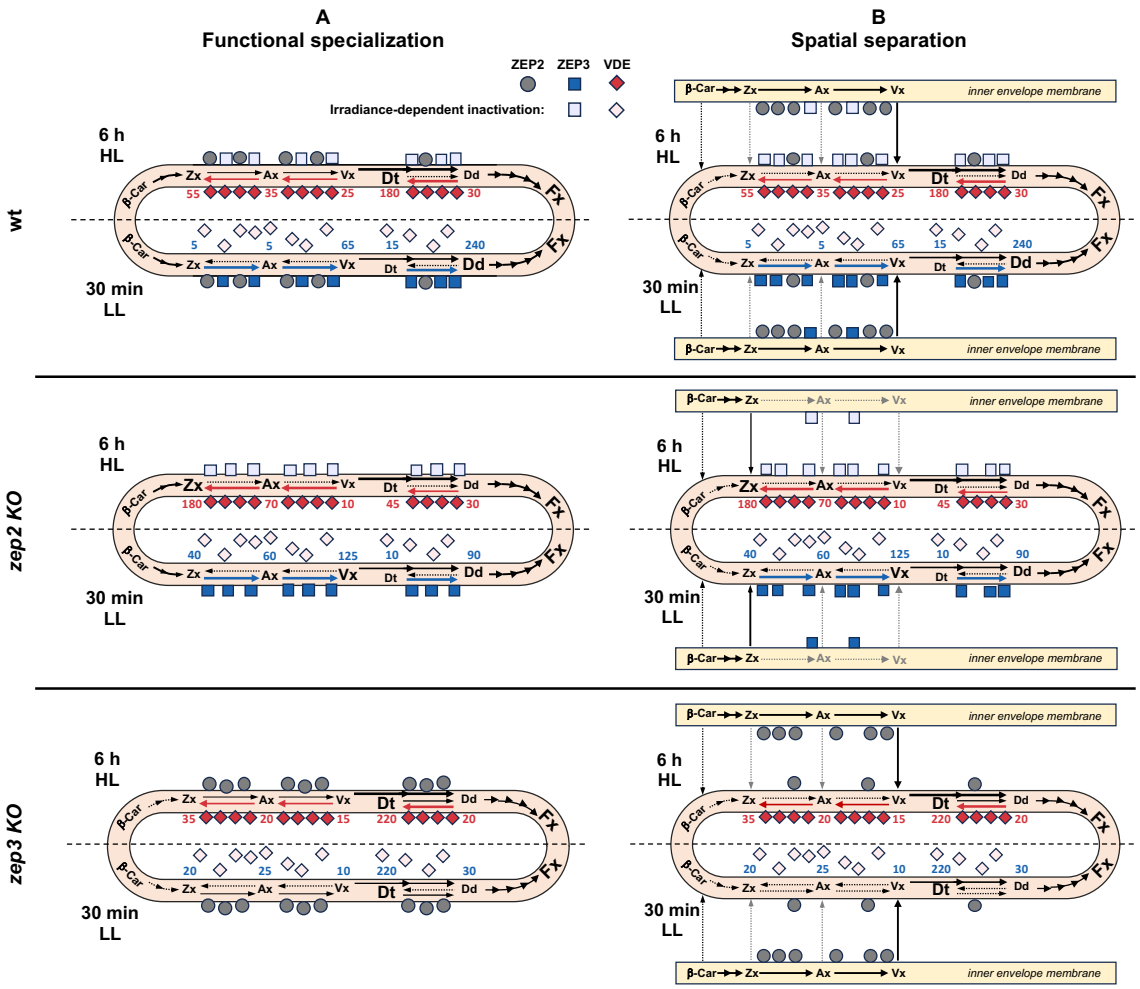

Fig. 6. Schematic models explaining the observed differences in xanthophyll accumulation between *zep2 KO*, *zep3 KO* and wt. Different panels show the state of each line at 6h of HL treatment (top) and after 30 min of recovery under LL (bottom). Colored arrows show preferential direction of xanthophyll cycles under HL (red) or LL (blue), numbers represent the relative concentration (xanthophyll:1000 chlorophyll *a*) of each xanthophyll cycle pigment at the corresponding time point. (*A*) Selective accumulation of Vx/Ax/Zx in *zep2 KO* could be explained by functional differences in the activity of ZEP2 and ZEP3. In this scenario, ZEP3 is selectively inactivated by HL while ZEP2 displays a lower but constitutive activity also under higher irradiances, thus causing lack of rapid Dt epoxidation in *zep3 KO* and accumulation of Vx/Ax/Zx in *zep2 KO*. (*B*) The two *zep* phenotypes could also result from the different localization of ZEP2 and ZEP3 in the chloroplast. In this model, ZEP2 is mostly located at the inner envelope, where it is responsible for the *de novo* synthesis of Zx and Vx. On the contrary, ZEP3 is confined mainly at the thylakoid membranes where it performs xanthophyll cycle-related Dt epoxidation.